# SENSOR CALIBRATION FOR CALCULATION OF LOADS ON A FLEXIBLE AIRCRAFT

## Marcus Vinicius P. Viana[1]

[1] Experimental fixed wing flight test engineer and PhD candidate at
DLR, Institute of Flight Systems, Lilienthalplatz 7, 38108 Braunschweig, Germany
marcus.preisigheviana@dlr.de

**Keywords:** Structural Health Monitoring (SHM), flexible aircraft, loads measurement, sensor calibration, structural load models, strain gauges, optical fibers, FBG (Fiber Bragg Grating).

**Abstract:** In order to reduce costs of operation, new aircraft designs make vast use of light, flexible, and slender structures to achieve higher payloads and improved fuel consumption. At the same time, in order to reduce the amount of flight testing required for the certification of a new aircraft, the use of simulation models for certification purposes increases constantly. These models must be validated based on real flight data, for which airplanes must be instrumented adequately. Nowadays the test setups available for strain sensor calibration are highly sophisticated and instrumented, but also complex, time-demanding and expensive. Therefore, the ability to provide cost effective methodologies will be of great benefit with regards to the often overlooked and ever growing flexible small aircraft market. The current paper focusses on the strain sensor calibration methodology for both strain gauges and Fiber Bragg Grating sensors. The methodology is presented with many details and illustrated using a real application to the DLR Discus-2c sailplane. Various practical pitfalls are discussed as well as the issue of selecting the "best" combination of sensors for the development of the local structural load models.

## 1 INTRODUCTION

The measurement of structural loads on an aircraft in flight plays a crucial role for the certification of new airplanes. In CS 25.301 [1], it is established that "methods used to determine load intensities and distributions must be validated by flight load measurements unless the methods used for determining those loading conditions are shown to be reliable". The goal of the flight test loads program is to demonstrate the load calculations and validate that the prediction process produces reliable loads for the flight certification cases [2]. Other applications for in-flight measurement of flight loads exist: these measurements can for instance also be used for aircraft structural health monitoring (SHM). The focus of this paper is to present a practical methodology, considering a restricted experimental scenario (e.g. limited budget and material support for a small aircraft), developed to allow the calculation of flight-loads based on a set of strain gauges and/or Fiber Bragg Grating (FBG) in order to provide accurate local information for the development and validation of structural loads and flight dynamics models of a flexible aircraft. The parameters of the loads equations are derived via a least-squares curve fitting algorithm using the strain gauge or optical fiber responses to a series of known point loads applied to the structure [3]. Important practical issues related to this sensor calibration process are addressed in this paper based on the example of the calibration performed for Discus-2c sailplane of DLR. In this context, it is presented with great detail the methodology that was used to determine the relationships

between the sensors that provide local information about structural loads, enabling flight-loads monitoring and validation. The development of the regression loads model is detailed and the best selection of aircraft sensors is analyzed and discussed based on statistical regression model quality measures. Problems such as irrelevant and redundant sensors during the loads model development are also addressed. The quality of the loads equations can be deduced from a comparison between results from different sources (or technologies) and from dedicated check loads.

In this context the loads model development process can be compared to the system identification approach [4]. As the current model building process pursues the best mathematical model; which contains unknown parameters that need to be determined indirectly from the measured data. A model providing a meaningful and accurate physical representation of the physical phenomena is searched, while being as simple as possible and providing insight to the engineers (no black-box model). These requirements are antagonist and therefore the corresponding model development requires making a compromise between them.

## 2 METHOD

### 2.1 Physical modelling

#### 2.1.1 General modelling and calibration of strain gauges

Skopinski [3] established that the relationship between the strain gauge bridge output $\mu$ and the structural loads (shear force $V$, bending moment $M$ and torque $T$) on a surface outboard of that bridge can be modelled with sufficient precision by a linear equation with coefficients $\alpha_V$, $\alpha_M$ and $\alpha_T$. In a typical calibration involving $j$ bridges and $n$ different calibration load cases, the output $\mu_{ki}$ of the $i$-th sensor to the k-th load case (defined by $V_k$, $M_k$, $T_k$) follows the following equation:

$$\forall(k,i) \in [\![1,n]\!] \times [\![1,j]\!] \,, \ \mu_{ki} = \alpha_{V,i}\,V_k + \alpha_{M,i}\,M_k + \alpha_{T,i}\,T_k \tag{1}$$

The linearity assumption implies that the principle of superposition can be applied, leading to consider that the strain at a particular location due to loads applied simultaneously to several points on the structure is the algebraic sum of the strains due to the same loads applied individually, a shear value $V$ applied at some point with coordinates $x$, $y$ would have a bending moment $M = V*y$ and torque $T = V*x$. Substituting these equations into equation (1), and extending it by inclusion of additional terms involving the coordinates and using the inverse relation, a linear function of the outputs of $j$ bridges is:

$$\{Vx^r y^s\} = [\alpha]^{-1}[\mu] \Rightarrow \forall k \in [\![1,n]\!], \ \begin{Bmatrix} V_k \\ M_k \\ T_k \end{Bmatrix} = \begin{bmatrix} \beta_{V,1} & \beta_{V,2} & \cdots & \beta_{V,j} \\ \beta_{M,1} & \beta_{M,2} & \cdots & \beta_{M,j} \\ \beta_{T,1} & \beta_{T,2} & \cdots & \beta_{T,j} \end{bmatrix} \begin{Bmatrix} \mu_{k1} \\ \mu_{k2} \\ \vdots \\ \mu_{kj} \end{Bmatrix} \tag{2}$$

Where { } represents a column vector; [ ] a matrix; [ ]$^{\mathrm{T}}$ the transpose of a matrix; [ ]$^{-1}$ the inverse of matrix; and the superscripts (r,s) = (0,0) for shear force, (1,0) for torque and (0,1) for bending moment. Considering that $j$ bridges are available and $n$ calibrated loads are applied, the least-squares normal equation can be obtained, enabling the determination of the load coefficients $[\beta_{\{V,M,T\},i}]$ by solving the following system of $j$ equations:

$$\Xi^T \begin{Bmatrix} V_1' \\ V_2' \\ \vdots \\ V_n' \end{Bmatrix} = \Xi^T \Xi \begin{Bmatrix} \beta_{V,1} \\ \beta_{V,2} \\ \vdots \\ \beta_{V,j} \end{Bmatrix} \overset{(when \ \Xi^T\Xi \ invertible)}{\Longleftrightarrow} \begin{Bmatrix} \beta_{V,1} \\ \beta_{V,2} \\ \vdots \\ \beta_{V,j} \end{Bmatrix} = [\Xi^T\Xi]^{-1}\Xi^T \begin{Bmatrix} V_1' \\ V_2' \\ \vdots \\ V_n' \end{Bmatrix} \quad (3)$$

$$\text{where } \Xi = \begin{bmatrix} \mu_{11} & \mu_{12} & \cdots & \mu_{1j} \\ \mu_{21} & \mu_{22} & \cdots & \mu_{2j} \\ \vdots & \vdots & \ddots & \vdots \\ \mu_{n1} & \mu_{n2} & \cdots & \mu_{nj} \end{bmatrix}$$

Applying $n$ different loads with known shear values $V_n'$ at $n$ different loading points, $n$ values of bending moment and torque are provided by the equations $M = V*y$ and $T = V*x$, allowing the determination of the values of $\{\beta_{M,i}\}$ and $\{\beta_{T,i}\}$ in equation (2), which are required to evaluate the bending moment and torque (load) equations. The least-squares solution equation (3) exists only if determinant of $[\Xi^T\Xi]^{-1}$ is greater than zero, which requires that the bridges with similar response characteristics should not be used together in a same load equation determination.

### 2.1.2 Fiber Bragg Grating (FBG) strain measurement principles

FBG work as a wavelength selective mirrors reflecting a narrow band of wavelengths. An illuminated FBG will reflect a narrow band spectral component corresponding to the Bragg resonance wavelength of the grating ($\lambda_B$), while all other wavelengths outside the narrow reflection band will be transmitted. FBG measurement technology relies on the principle that any change of the FBG period and/or the refractive index result in a modification of the reflected Bragg wavelength $\lambda_B$. A FBG responds to some physical parameters such as temperature ($\Delta\lambda_B \propto K_{TEMP} * \Delta TEMP$) and mechanical strain ($\Delta\lambda_B \propto K_{strain} * \Delta strain$). Considering a mechanical strain applied to a FBG, expansions and compressions of the grating region will occur, thus changing the FBG period resulting in a modified refractive index [5].

## 2.2 Statistical tools and metrics

Before describing in more details the complete calibration methodology, a few statistical tools and metrics that are used in this methodology are introduced hereafter.

### 2.2.1 Statistical metrics of quality of Multiple Ordinary Least-Squares (OLS) regression and of Regression Through the Origin (RTO)

The traditional analysis of variance decomposition for the OLS case is expressed by:

$$\sum_{k=1}^{n}(Y_k - \bar{Y})^2 = \sum_{k=1}^{n}(Y_k - \hat{Y}_k)^2 + \sum_{k=1}^{n}(\hat{Y}_k - \bar{Y})^2 \Rightarrow SST = SSE + SSR \quad (4)$$

Where $Y$ are the response measurements, $\hat{Y}$ are the fitted values, SST is the sum of squares total, SSE is the sum of squares due to error and SSR is the sum of squares due to regression. Thus, the OLS multiple coefficient of determination is defined by the ratio of SSR and SST:

$$R^2 = \frac{SSR}{SST} = \frac{\sum_{k=1}^{n}(\hat{Y}_k - \bar{Y})^2}{\sum_{k=1}^{n}(Y_k - \bar{Y})^2} \quad (5)$$

3

This metric of quality of the fit measures the proportion of variation in the dependent variable that is explained by the dependent variable´s relationship to all the independent variables in the model. However, in order to compare different models with different numbers of predictors, $R^2$ is not a sensible criterion to select the best model, because it does not penalize the excessive use of unimportant independent variables.

Regression through the origin is a special case of ordinary least-squares (OLS) regression, where the intercept (constant term) is zero. As mentioned by Eisenhauer [6], the RTO residuals will usually have a nonzero mean, due to the fact that forcing the regression curve through the origin causes generally incompatibility with the best fit. The inappropriate use of the $R^2$ expression obtained for the OLS case can lead to an uninterpretable negative value of coefficient of determination as well as negative F ratio [6]. Therefore, in the case of a regression through the origin, equation (5) takes the form expressed by equation (6). It is obvious these new definitions influence the adjusted $R^2$ and, F and t statistics, but the sum of squared error (SSE) and the standard error of the regression ($\sqrt{MSE}$) remain unchanged, except by the change of number of degrees of freedom.

$$R^2 = \frac{SSR}{SST} = \frac{\sum_{k=1}^{n} \widehat{Y}_k^2}{\sum_{k=1}^{n} Y_k^2} \tag{6}$$

### 2.2.2 Additional metric of quality for general multiple linear regression models

As addressed by Yan et al. [7], the Akaike Information Criterion (AIC) is derived from information theory as a data-based approximation for the Kullback-Leibler discrepancy function between a candidate model and the true model. The approximation in equation (7) is possible for Gaussian or normal models [7]:

$$\begin{aligned} AIC &= n * \log(likelihood) + 2 * p \\ &\approx n * \log(SSE) + 2 * p \end{aligned} \tag{7}$$

The interpretation for this formula is that the first term measures the quality of fit of the regression model, penalized by model complexity depicted in the second term 2 p, which is frequently denominated as complexity or penalty parameter [7] and the coefficient 2 was selected by Akaike in his formulation development [8], [9]. So the model selection is adjusted by penalizing complex models with several predictors that do not fit much better than simpler models with fewer predictors. Therefore a smaller AIC represents better potential model [7]. This alternative approach is suitable to measure the quality of fit of OLS regressions as well as regressions through the origin (RTO), taking into account the number of regressors included in the potential model.

As a summary, taking into account large samples, a model selection criterion could be classified as efficient, when the model with minimum mean squared error (MSE) is pursued, or consistent, when the true model with probability one is selected. There is no criterion that satisfies both characteristics. In this context, MSE, adjusted $R^2$ and AIC are all asymptotically efficient criteria while BIC (Bayesian Information Criterion) is a consistent one [7]. It is advised that AIC is suitable for moderately-sized sample and BIC is most suitable for large samples with relatively strong signals [7]. In the AIC approach, the candidate models are straightforward classified from best to worst based on the available empirical data. AIC is a simple and compelling metric, based on deep theoretical foundations as entropy, Kullback-

Leibler information and likelihood theory. In this sense, the model development is pursued by the minimization of the information loss, separating the noise (entropy or residuals) from the data signal. That is, the efforts are not to model the data, but the model is developed by the modeling of the information contained in the data [8]. This issue about the optimization criterion will be addressed in a little more detail in section 4.5.

### 2.2.3 Standard statistics applied to Multiple Ordinary Least-Squares regressions (OLS)

Due to the fact that the regression model is built based on a sample of data from the population, being subject to sampling error, it is necessary to test the statistical significance of the overall regression and also each estimated coefficients of the regression model. The F-test statistic is used to evaluate the overall significance of the model. Large values of F indicate a bigger evidence that the regression model explains a significant portion of the variation in $Y$ (i.e. at least one independent variable affects $Y$). To solve the problem of irrelevancy, the t-test statistic is useful to determine the individual predictor significance. This test verifies if there is a linear relationship between each specific predictor and $Y$. One observation about the F-test and t-test statistics (p-value) as well as the previously presented OLS $R^2$ and adjusted $R^2$ is that these approaches are evaluated under the assumption that the model has a constant term (intercept). So, it is not correct to apply these statistical approaches for regressions through the origin (RTO) and perform a straightforward comparison with the OLS results.

### 2.3 Methodology used

The strain measurement sensors, namely FBG and strain gauges, were calibrated by a specific ground calibration procedure [10]. The objective of this sensor calibration was to enable the calculation of loads on a flexible aircraft through the strain measurements. To fulfill this objective, a comprehensive calibration setup was planned and performed considering the different type of loads to be measured and the respective number of sensors and their positions. The calibration has pursued to cover a significant and optimal range of positions and magnitudes of loads that could be experienced during flight, in order for the loads equation to be able to determine the flight loads later on and avoiding extrapolations due to unaddressed load cases. A series of suitable and known loads were applied at different chordwise and spanwise positions. The magnitude of these loads was varied and did cover the range of loads that shall be expected in flight.

After performing the calibration tests and gathering the strain sensor measurements, the model building is the process of selection of predictors in order to include only the significant predictors, which are informative about the measurement response $Y$. The aim is to build a reliable regression model that fits the data well and predicts loads well in practice, while being as simple as possible. As pointed out by Sauerbrei et al. [11], model selection in general is still an open question. Although advances in the computational power and statistical sophistication permits to fit almost a model to any dataset, obtaining a "good" model is not a straightforward task. On the one side, a simple model can present smaller variance of the approximation error, but with biased or inaccurate estimation, but on the other hand a complex model can provide unbiased estimation or better quality of fit to the data, but with larger variance or imprecise estimation [7]. Considering that there are two possibilities for each regressor (each strain sensor can be either included or omitted), in the case of $j+1$ regressors, $(2^{j+1} - 1)$ potential subsets will exist (excluding the null model with the intercept term only). The methodology of the present work for model building is divided into two parts:

1. First, all combinations of predictors that provide OLS regression models are evaluated. The predictors that include the intercept (constant term different of null) are subjected to the F-test statistic to check if the OLS regression model is able to explain a significant portion of the variation in the load. One of the benefits of using the least-squares solution for the determination of load coefficients is the possibility of stipulating the reliability and relevancy of any equation by standard statistical methods. Thus, considering that the expansion of the RTO shear expression in equation (2) requires j bridges and the load coefficients $\beta_{V,0}, \beta_{V,1}, \beta_{V,2}, \ldots, \beta_{V,j}$ were obtained by least-squares, a OLS shear preliminary calibration equation $V_{preliminary}$ $(\beta_{V,0} \neq 0)$ can be represented by:

$$V_{preliminary} = \beta_{V,1}\mu_1 + \beta_{V,2}\mu_2 + \cdots + \beta_{V,j}\mu_j + \beta_{V,0} \tag{8}$$

In the case of equation (8), $\beta_{V,2}$ is the coefficient with the largest magnitude and $\beta_{V,0}$ is the intercept term. Performing the factorization of equation (8), the OLS shear final calibration equation $V_{final}$ can be obtained, being a direct measure of shear alone:

$$V_{final} = \beta_{V,2}\left(\frac{\beta_{V,1}}{\beta_{V,2}}\mu_1 + \mu_2 + \cdots + \frac{\beta_{V,j}}{\beta_{V,2}}\mu_j + \frac{\beta_{V,0}}{\beta_{V,2}}\right) = \beta'\rho_V \tag{9}$$

Passing this first test, in the second stage the coefficients are evaluated by the t-test statistic, where their individual significances are checked. The t-values and p-values provide a guide for making decisions about selecting determined combination as a candidate model. If any coefficient does not pass this t-test statistic, the combination is rejected. If the intercept coefficient $\beta_{V,0}$ is significant, the selection of the best model is reached by the set of coefficients that provides the highest adjusted $R^2$, the lowest standard error of the load, the lowest Akaike Information Criterion (AIC), the lowest Bayesian Information Criterion (BIC) and the highest F value. In case it is impossible to satisfy all these conditions (criteria for measuring the quality of estimation) at the same time, an architecture of hierarchy (i.e. a list of priority between these different optimization criteria) has been developed in order to reach the desired model.

2. The second part of the methodology is only applicable in the case when the intercept coefficient $\beta_{V,0}$ is classified as insignificant in the t-test statistic. In this situation $(\beta_{V,0} = 0)$, the model is obtained by a regression through the origin (RTO). Therefore all combinations of potential (i.e. not previously rejected) predictors in a RTO are fitted and the selection of the best model is achieved by the optimization of two different criteria: smallest standard error of the load and the lowest AIC.

Equations (8) and (9) represent the preliminary and final shear load equations, respectively. Similar load equations can be obtained for the bending moment and torque. The $\beta'$ final coefficients (also evaluated by least-squares) are determined by a final calibration (recalibration) through the application of a set of calibrated loads at different chordwise and spanwise locations as in the preliminary equation. This final calibration should include both symmetrical and asymmetrical loading conditions. Summarizing each explained part of this methodology is applied separately for each load type (shear, torque and bending moment) at each load station for each calibration step (preliminary and final calibrations). The difference is that each preliminary load equation uses only the shear and bending moment sensors installed at its specific load station and each final load equation uses combinations of final shear, torque and bending moment sensors installed at any load station (see the next paragraph and equation (10) for more details).

If the number of installed bridges is limited, the use of the previous explained procedure (see equations (8) and (9)) can restrict the number of loads which are possible to be measured. In this case, Skopinski [3] suggests to apply a procedure in which the data obtained during preliminary and final calibrations are used to combine bridges with the same primary sensitivity, that is, the shear-sensitive bridges on one side of the structure are combined into a single channel, the moment-sensitive bridges on one side into a single channel and torque-sensitive bridges into a single channel. This approach was adopted in the methodology used in this work. Finally the following OLS final calibration equation (compare with equation (9)) is acquired, for a simple example considering only one load station at each wing (L: left wing load station; R: right wing load station):

$$
\begin{Bmatrix} V_L \\ M_L \\ T_L \\ V_R \\ M_R \\ T_R \end{Bmatrix}_{final} =
\begin{bmatrix}
\beta'_{V_L,0} & \beta'_{V_L,\rho_{V_L}} & \beta'_{V_L,\rho_{M_L}} & \beta'_{V_L,\rho_{T_L}} & \beta'_{V_L,\rho_{V_R}} & \beta'_{V_L,\rho_{M_R}} & \beta'_{V_L,\rho_{T_R}} \\
\beta'_{M_L,0} & \beta'_{M_L,\rho_{V_L}} & \beta'_{M_L,\rho_{M_L}} & \beta'_{M_L,\rho_{T_L}} & \beta'_{M_L,\rho_{V_R}} & \beta'_{M_L,\rho_{M_R}} & \beta'_{M_L,\rho_{T_R}} \\
\beta'_{T_L,0} & \beta'_{T_L,\rho_{V_L}} & \beta'_{T_L,\rho_{M_L}} & \beta'_{T_L,\rho_{T_L}} & \beta'_{T_L\rho_{V_R}} & \beta'_{T_L,\rho_{M_R}} & \beta'_{T_L,\rho_{T_R}} \\
\beta'_{V_R,0} & \beta'_{V_R,\rho_{V_L}} & \beta'_{V_R,\rho_{M_L}} & \beta'_{V_R,\rho_{T_L}} & \beta'_{V_R,\rho_{V_R}} & \beta'_{V_R,\rho_{M_R}} & \beta'_{V_R,\rho_{T_R}} \\
\beta'_{M_R,0} & \beta'_{M_R,\rho_{V_L}} & \beta'_{M_R,\rho_{M_L}} & \beta'_{M_R,\rho_{T_L}} & \beta'_{M_R,\rho_{V_R}} & \beta'_{M_R,\rho_{M_R}} & \beta'_{M_R,\rho_{T_R}} \\
\beta'_{T_R,0} & \beta'_{T_R,\rho_{V_L}} & \beta'_{T_R,\rho_{M_L}} & \beta'_{T_R,\rho_{T_L}} & \beta'_{T_R,\rho_{V_R}} & \beta'_{T_R,\rho_{M_R}} & \beta'_{T_R,\rho_{T_R}}
\end{bmatrix}
\begin{Bmatrix} 1 \\ \rho_{V_L} \\ \rho_{M_L} \\ \rho_{T_L} \\ \rho_{V_R} \\ \rho_{M_R} \\ \rho_{T_R} \end{Bmatrix} \quad (10)
$$

As suggested by Kvålseth [12] and Eisenhauer [6], a precautionary approach was adopted in the current work, considering initially the problem as an OLS regression and applying the p-values (Student's t-test statistic) for the OLS constant. If the significance of this constant is low and does not pass in the mentioned test, the use of a regression through the origin (RTO) is justified. In the last part of the process to select the best load equation, the standard errors of the OLS and RTO are compared in order to define the final fit quality. This precautionary approach states that zero-intercept models (RTO) should only be used when both theoretical justification and empirical data analysis indicate that they are indeed appropriate [12]. The final set of coefficients in the best load equation is determined by evaluating all the possible combinations of the available sensors in each stage of the preliminary and final calibrations. As already mentioned, in the current work, all possible combinations are analyzed instead of dropping or adding the bridges one by one and recalculating the coefficients, as performed for example by the backward and forward selection methods of [7] and [11]. The final task when building a multiple linear regression model is to evaluate how well it performs. From the plot of the residuals, several analyses can be visually made, such as the check of the aptness of the model and the goodness of fit.

The contribution of this methodology is to enable the development of a reconfigurable health monitoring system. The robustness, sensitivity, degradation and long term stability of the strain sensors can be constantly monitored by the cross check and cross validation of each load in each load station through different load equations. The probable errors of the estimates of a specific load from different load equations are used to verify if there is intersection between their load predictions in a specific position. In the case of disagreement of any load estimate with the other estimates, this questionable load equation is neglected in order to exclude this faulty strain sensor from the loads monitoring system. Subsequently, a valid model for this specific load becomes effective on the health monitoring system, restoring the ability of predicting an accurate load on this airframe position. Therefore this process of auto check, monitoring and validation of the loads predictions provides an enhanced capability of reconfiguration and reparability of the SHM system associated with high levels of reliability and robustness. As a final contribution of this current methodology is the calibration of

different types of strain sensors installed in different structural aircraft components (like wings and horizontal tailplane) in several spanwise positions in order to prove the feasibility and reliability of practical applications of structural loads monitoring systems.

## 3 APPLICATION CONSIDERED

### 3.1 Aircraft description – test platform

The Discus-2c is a single-seat high performance sailplane manufactured by Schempp-Hirth Flugzeugbau GmbH. The sailplane is constructed from fiber reinforced plastic (FRP), featuring a T-tail, as shown in Figure 1. The DLR Discus-2c has a wing span of 18 meters and additional information is presented in Table 1.
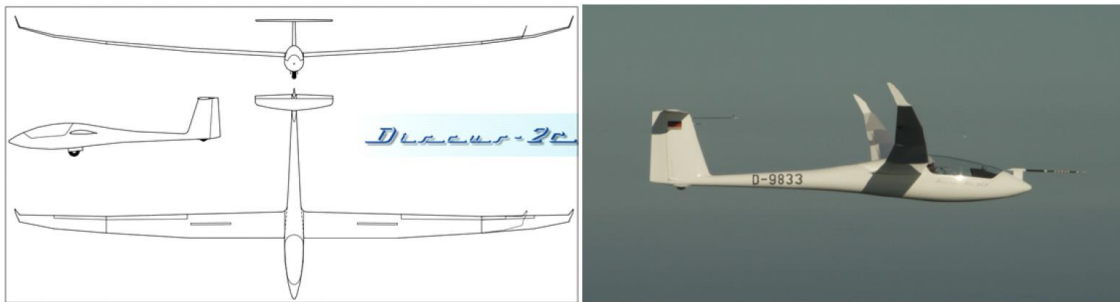


Figure 1: DLR Discus-2c

| Wing | | Fuselage | | Mass (kg) | |
|---|---|---|---|---|---|
| Span (m) | 18 | Length (m) | 6.78 | Empty mass approx. | 280 |
| Area (m$^2$) | 11.39 | Width (m) | 0.62 | Maximum all-ups mass | 565 |
| Aspect ratio | 28.5 | Height (m) | 0.81 | Maximum water ballast | 200 |
| Mean aerodynamic chord - MAC (m) | 0.685 | | | Wing loading (kg/m$^2$) | 31.2 – 50.0 |

Table 1: Discus-2c technical data

### 3.2 Test instrumentation for the strain sensor calibration
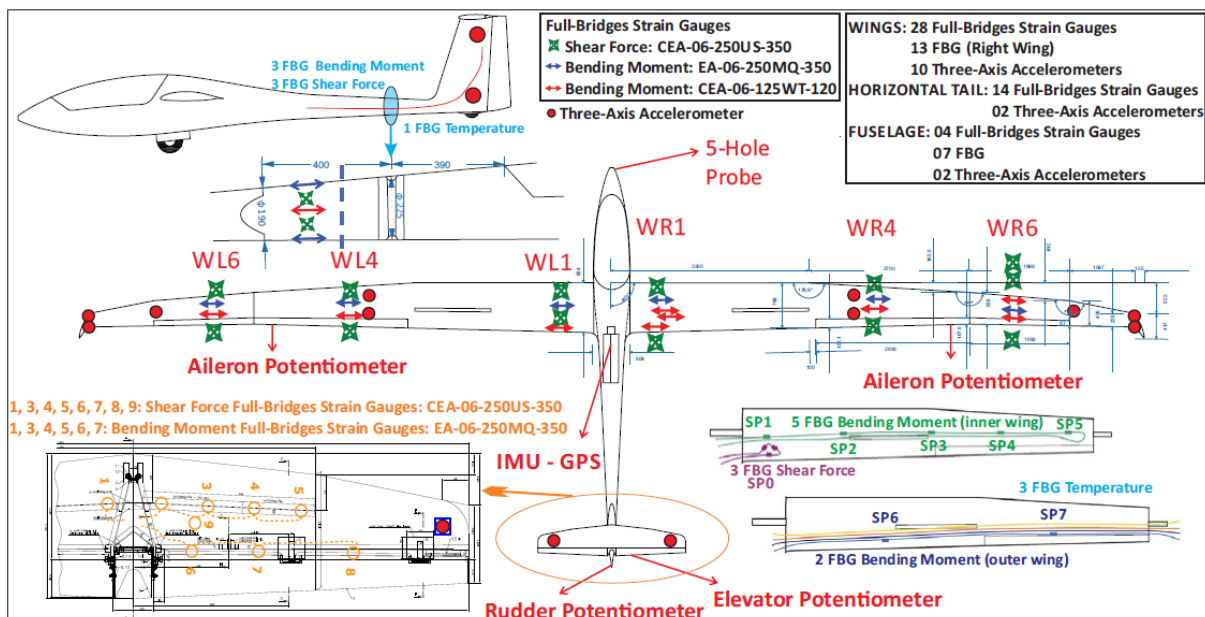


Figure 2: Specialized structural flight test sensors installed on Discus-2c sailplane

8

For developing a structural loads monitoring system, spread at different aircraft positions, 20 optical fibers (FBG) were installed to measure calibrated flight loads. Additionally, to validate the structural-loads calculations from the FBG and also for structural displacement measurements, 46 four-active-arm strain gauges were placed on strategic internal aircraft stations. The complete instrumentation setup for the structural model identification purpose, i.e. measurements of the modal displacements, modal accelerations, modal shapes and structural loads, is illustrated in Figure 2 and Figure 3, and detailed in Table 2.

| Aircraft Structure | Strain Sensor | Load Sensitivity | Spanwise Position (W and HT) or x-axis Position behind the ring frame (FUS) | Architectures of full-bridge strain gauges / characteristic FBG wavelength |
|---|---|---|---|---|
| Wing (W) | 3 FBG | Shear force | +663, +705 and 737 (SP0) mm | 1524.850, 1532.361 and 1540.672 nm |
| | 13 strain gauges | | ±820 (SP1), ±4400 (SP4) and ±6890 (SP6) mm | CEA-06-250US-350 (1x) |
| | 7 FBG | Bending Moment | +820 (SP1), +2010 (SP2), +3205 (SP3), +4400 (SP4), +5600 (SP5), +6890 (SP6) and +7885 (SP7) mm | 1523.918, 1532.972, 1542.893, 1552.832, 1562.860, 1524.121, 1533.060 nm |
| | 15 strain gauges | | ±820 (SP1), ±4400 (SP4) and ±6890 (SP6) mm | EA-06-250MQ-350 (2x) and CEA-06-125WT-120 (2x) |
| | 3 FBG | Temperature | +900, +4400 and +7300 mm | 1523.996, 1532.848 and 1543.071 nm |
| Rear Fuselage (FUS) | 3 FBG | Shear force | 300 mm behind the ring frame (SP3) | 1542.858, 1533.030 and 1564.238 nm |
| | 2 strain gauges | | 250 mm behind the ring frame (SP2) | CEA-06-250US-350 (1x) |
| | 3 FBG | Bending Moment | 150 mm behind the ring frame (SP1) | 1548.110, 1556.290 and 1562.923 nm |
| | 2 strain gauges | | 250 mm behind the ring frame (SP2) | EA-06-250MQ-350 (2x) and CEA-06-125WT-120 (2x) |
| | 1 FBG | Temperature | 300 mm behind the ring frame (SP3) | 1552.511 nm |
| Horizontal Tail (HT) | 8 strain gauges | Shear force | -120 (SP1), +230 (SP6), +240 (SP9), +267 (SP3), +414 (SP4), +475 (SP7), +560 (SP5) and +720 (SP8) mm | CEA-06-250US-350 (1x) |
| | 6 strain gauges | Bending Moment | -120 (SP1), +230 (SP6), +267 (SP3), +414 (SP4), +475 (SP7) and +560 (SP5) mm | EA-06-250MQ-350 (2x) |

Table 2: Characteristics of the flight test instrumentation for calculation of loads on a flexible aircraft

## 3.3 Calibration setup and test points

Nowadays the test setups available for strain sensor calibration are highly sophisticated and instrumented, as can be seen in [13], but also very complex and expensive. However, the aim of the current strain sensor calibration was to demonstrate how to perform a straightforward process with the simplest hardware. The work core was to develop a calibration test focused on a methodology that could be easily applied since on a basic sailplane until a complex modern large transport aircraft, using accessible equipment setup, without neglecting the quality of the results. In order to perform the calibration, the equipment test scenario was composed by the equipment presented in Table 3.
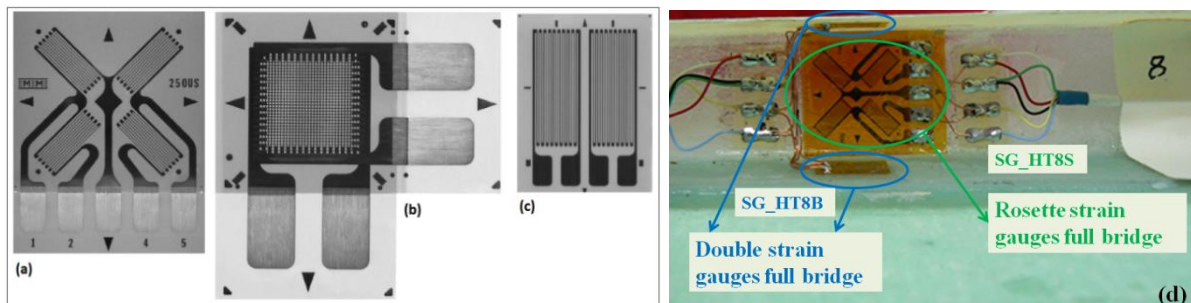


Figure 3: Strain gauge types used during this calibration test: (a) CEA-06-250-US-350 type (Rosette strain gauge); (b) CEA-06-125WT-120 type (T strain gauge); (c) EA-06-250MQ-350 type (Double strain gauge); (d) Standard setup for the strain gauge full bridges installation at the spar of the elevator

9

| Calibration Equipment |
|---|
| 25 sand bags to apply up and down loads over the wings and fuselage (as shown by Figure 4). Mass of each sand bag was between 11.71 and 12.03 kg, size: 30 x 60 cm |
| Metal bars to apply up and down loads over the horizontal tailplane |
| Rubberized fabrics to prevent damage to the aircraft surface |
| Clamp to apply torsion in the right wing (see Figure 4) |
| Trestle with foam at the top in order to avoid small wing oscillations and ease the stabilization of the wing after the load application and before the measurement recording |
| Prepared belts and crane to hold the aircraft in the upside down position (up loads) |
| Spirit level |
| Laser equipment to measure the vertical displacements of the wing and tailplane |
| Data Acquisition System: strain gauge four-active-arm bridges and optical fibers (FBG) |

Table 3: Equipment setup for the calibration of the strain sensors of the Discus-2c
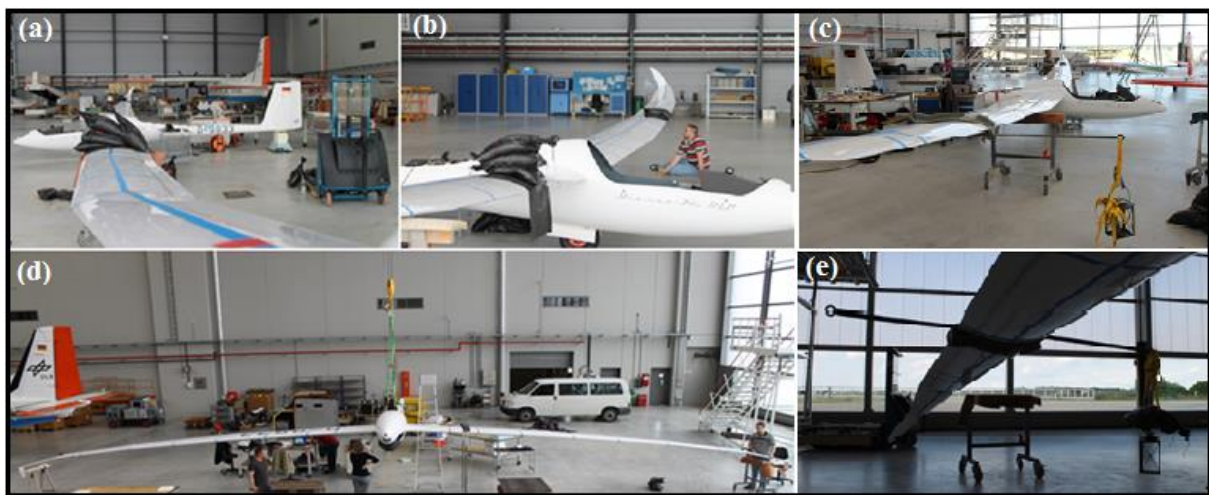


Figure 4: (a) (b) Down loads; (c) (e) Torque application using a specially designed clamp (aircraft in the normal and upside down conditions); (d) Up loads (aircraft held in the upside down condition by prepared belts)

During the period between of May 21$^{st}$ and of June 10$^{th}$ 2014, 46 four-active-arm strain gauge bridges installed on the wings, rear fuselage and horizontal tail; and 20 optical fibers (FBG) installed on the right wing and rear fuselage were calibrated. For the calibration of these load sensors 532 test points were performed, distributed as summarized in Table 4.

| Number of Load Cases | Aircraft Structure | Amount of Strain Sensors | Type of Load | Direction of Load Application |
|---|---|---|---|---|
| 303 | Wings | 28 strain gauges 13 optical fibers | - Symmetric and Asymmetric Shear and Torque<br>- Only Symmetric bending moment | Downward and Upward |
| 175 | Horizontal Tail | 14 strain gauges | - Symmetric and Asymmetric Shear and Torque<br>- Only Symmetric bending moment | Downward and Upward |
| 50 | Rear Fuselage | 4 strain gauges 7 optical fibers | - | Upward |
| 4 | Wings and Horizontal Tail | 42 strain gauges 13 optical fibers | - No load (components disassembled for the determination of the reference conditions) | - |

Table 4: Load cases performed for calibration of the load sensors

## 4 RESULTS AND ANALYSIS

### 4.1 Reference conditions for the strain sensor calibration

For a proper strain sensor calibration, the load cases are required to encompass the most comprehensive load spectra experienced during the flights. For the success of this work it was fundamental to consider a correct reference condition for each aircraft orientation, namely in the normal and upside down conditions, which should be measured in a stabilized condition on the ground with all aircraft components assembled and without external loads application. So strain sensors calibrated according to the methodology described in this paper calculate structural loads relative to these reference conditions. Figure 5(a) and Figure 5(b) show the plots between bending moment and the strain gauge response, respectively, without and with compensation based on the reference condition. Failure to consider the proper reference conditions would prevent from properly interpreting the sensor measurements and from determining the applied loads.
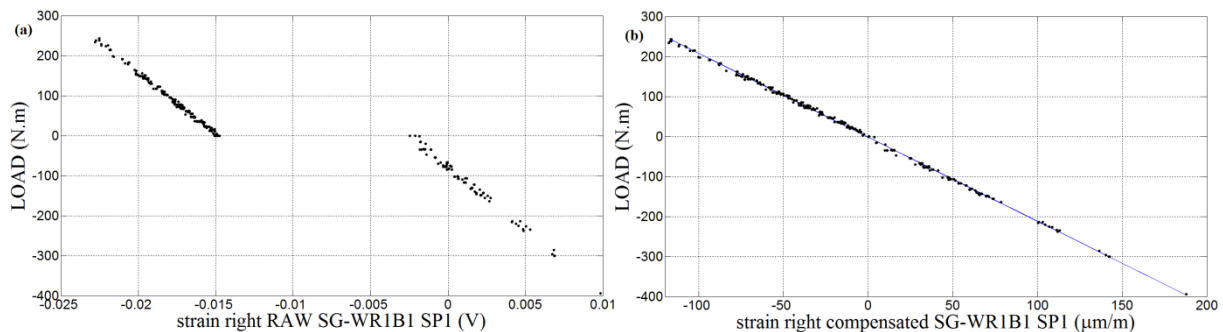


Figure 5: Strain gauge responses of the SG-WR1B1 sensor from the applied bending moment: (a) without a reference condition; (b) taking into account a reference condition

### 4.2 Transformation of FBG sensor measurements in pure mechanical strains
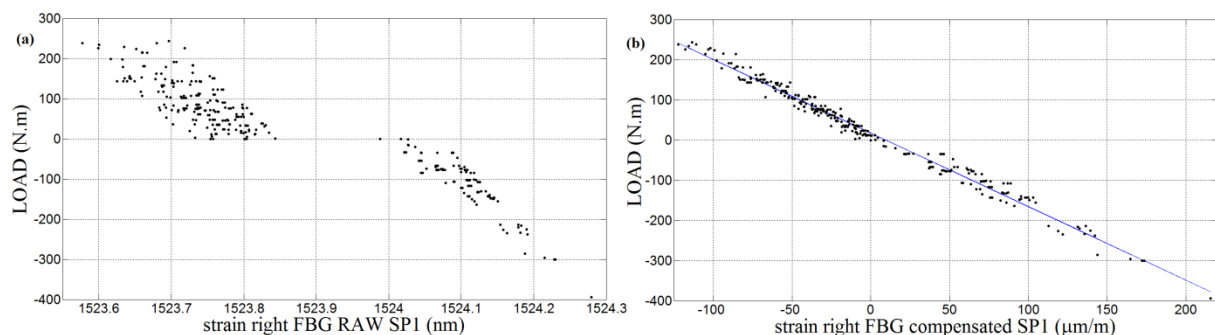


Figure 6: (a) Raw FBG sensor measurements at the right wing spanwise 1 (bending moment load cases); (b) Compensated FBG sensor measurements at the right wing spanwise 1 (bending moment load cases)

During the analysis of the optical fiber measurements, considerable variation of the wavelength values plotted against the applied loads was verified, as shown in Figure 6(a). A well-known fact that could be verified during the FBG calibration is that the temperature effects are important and the strain measurements need to be corrected accordingly. In order to be able to correct this effect, the temperature was measured during all the calibration tests. Even for the relatively small temperature changes that were experience during the calibration (less than 7°C), the strong influence of the temperature on the strain measurements was

clearly noticeable. Note that the temperature variations are expected to be significantly larger in flight than during the calibration, which would lead to even stronger variations of the strain measurements. Considering the outputs of the FBG temperature sensors and their references, the contribution of the temperature changes into the strain values can be subtracted, leading to a pure structural deformation caused by only the known applied loads. At the end, a well-defined relationship between aircraft deflections and applied loads was obtained, as shown in Figure 6(b).

**4.3 Influence of the structural position on the sensor sensitivity**

One important topic of this work was to investigate the influence of the structural position of the strain gauge sensors on their strain sensitivity. 28 strain gauge sensors were installed on the wings. The 303 load cases applied at the wings were used to conduct this analysis. The scope of this investigation encompasses the relation between the type of the strain gauge sensor and its structural position with the quality of the load sensitivity regarding shear force, bending moment and torque. There are three types of strain gauge sensors installed at the wings, shown by Figure 3. For shear force and torque measurements the strain gauge CEA-06-250-US-350 type, also called as Rosette strain gauge, was used. Only one set of this strain gauge type is necessary to compose a full bridge. There are two options for bending moment measurements. First, the CEA-06-125WT-120 type, also called T strain gauge, was used twice either on the lower or upper shell internal surface to compose a full bridge. The second option is the EA-06-250MQ-350 type (called as double strain gauge), where two sets are required to constitute a full bridge. Thereby, one set was installed on the upper surface and the other on the lower surface.
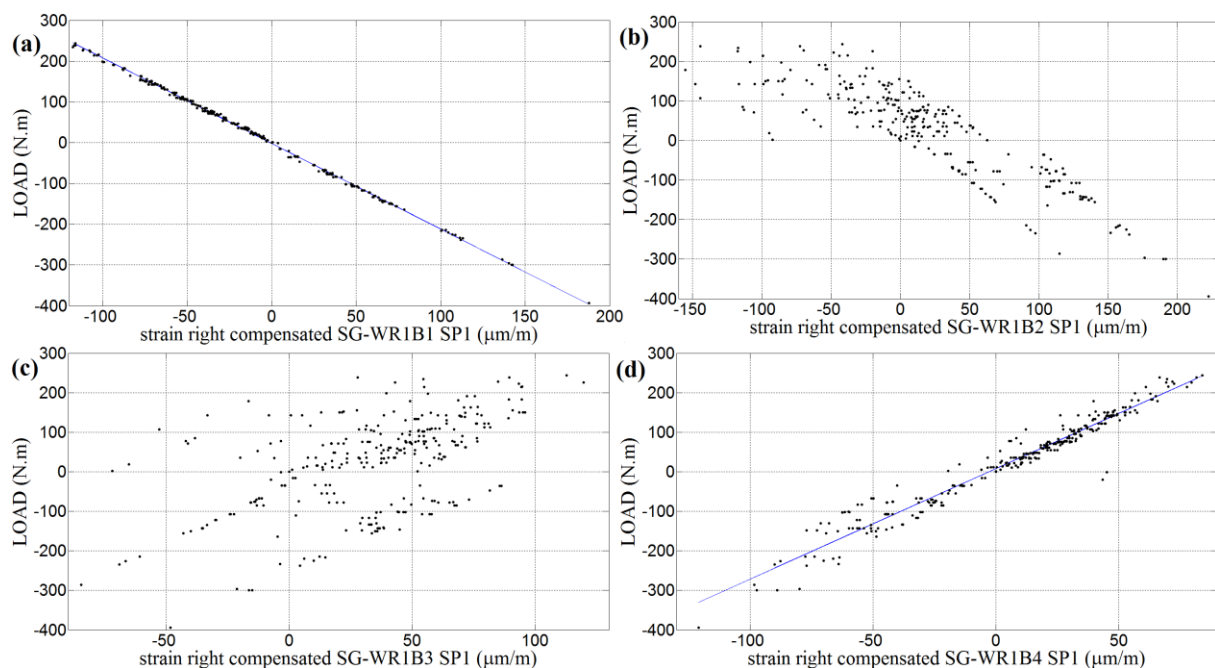


Figure 7: Relationship between the applied bending moments and the strain measurements from the sensors installed at the right wing in the spanwise 1: (a) sensor SG-WR1B1 (double strain gauge) at the spar; (b) sensor SG-WR1B2 (T strain gauge) at the spar; (c) sensor SG-WR1B3 (T strain gauge) at the spar; (d) sensor SG-WR1B4 (T strain gauge) at the inner side of the wing lower shell (behind the spar)

There are six strain gauge full bridges installed at spanwise location #1 (SP1 or WR1, see Figure 2) of the right wing that encompass the three available types. These sensors are positioned in three different chordwise locations. There are four sensors for bending moment

measurements in two different chordwise, one over the wing spar and other behind the spar. Starting the analyses with the two sensor types on the wing spar, one can verify that the double strain gauge type (EA-06-250MQ-350 – sensor SG-WR1B1) has enhanced sensitivity for bending moment. The other type (T strain gauge or CEA-06-125WT-120) installed at the spar, represented by the sensors SG-WR1B2 and SG-WR1B3, present significant scatter, showing small or apparently negligible sensitivity for bending moment measurements. However, installing this type of sensor (in this case named as SG-WR1B4) on the wing shell (out of the stiff wing spar), its sensitivity becomes noticeable, but still smaller than that for the EA-06-250MQ-350 type. These evaluations are provided by the analyses of Figure 7. Another important investigation is the verification of how well the four-active-arm architecture of a strain gauge full bridge works in compensating the temperature effects on the strain measurements. Comparing Figure 6(b) and Figure 7(a), it can be concluded that the strain gauge sensors cancel the thermal effects on the strain measurements quite well.

Considering the shear force and torque sensitivities, there is only one type of sensor, CEA-06-250-US-350 or Rosette strain gauge, installed in two main different chordwise positions: wing spar (vertical web) and wing shell (in different horizontal positions). The sensor installed in the vertical web (SG-WR1S1) presents better sensitivity than that installed on the horizontal wing shell (SG-WR1S2). However, in this case, the sensor installed in the horizontal wing shell provides a meaningful signal that represents a mix of shear force and torque measurements.

The previous observations provide valuable information permitting to select sensor locations which are well suited for the development or the validation of a load model. The correct choice of the sensor types and their positions on the structure are key drivers for the success or the failure of any calibration almost regardless how sophisticated is the employed calibration technique itself. Other important issues are that the compounding of different information sources from different sensor types installed in different structural locations can be important for the development of comprehensive loads models, even if the plots of the sensor outputs against the applied loads seem to be not meaningful at first glance. This results from the fact that the coupling between different load types may not be easily identified by a graphical analysis from the strain sensor outputs against the applied load cases. This issue can be demonstrated by the preliminary load models that use these apparent weak signals to constitute the loads equations. That is, the methodology proposed in this paper identifies these apparent secondary sensors as essential to compose a more accurate loads equation. Therefore, the results of these evaluations provide a valuable guide for the practical applications where there is a restriction of the number of strain sensors that can be installed. So the priority is to install the most sensitive sensors for each type of load in the main structural locations as discussed previously. Afterwards, in the case of additional available strain gauges or optical fibers, these other sensor types applied to different structural locations can then be used in order to improve the accuracy and quality of the loads regression models, or to provide redundancy and cross-checking possibilities.

**4.4 Influence of number of strain sensors in the quality of the loads regression models**

From the calibration of the strain gauges and optical fibers sensors installed on the fuselage, important analyses can be done. In possession of these results, it is possible to investigate the minimum number of each sensor type-sensitivity necessary to develop a suitable load regression model. Figure 8 and Figure 9 contrast the differences between a final load regression model using three sensors for each type of load (3 FBG for shear and 3 FBG for

bending moment measurements) against another using only two sensors (2 strain gauges for shear and 2 strain gauges for bending moment measurements). It is clear from these plots and the values of probable errors of load estimates that the FBG load models have more power to explain the variation of shear force and torque separately than the strain gauge load models. Only two shear-type sensors are unable to decouple the influences of shear and torque on the respective individual torque and shear load models. Adding a third shear-type sensor improves the accuracies of both shear and torque regression models, as shown by the evolution of the quality of the fitted load models in Figure 8(a) to Figure 8(b) and Figure 9(a) to Figure 9(b), respectively.
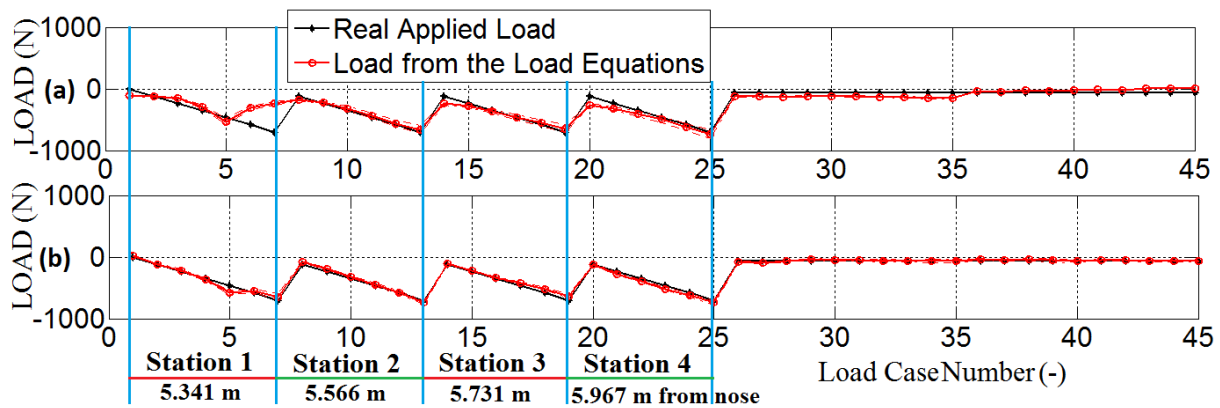


Figure 8: Final shear force load model determined from: (a) the strain gauge sensors (2 shear-type and 2 bending-moment-type); (b) the FBG sensors (3 shear-type and 3 bending-moment-type). Using all load cases

This investigation was possible due to the fact that the load application on the rear fuselage of the sailplane can provide a very close case of pure shear and torque loads. Because the load application did not have the possibility to drift so far from the sailplane centerline, due to the small width of the rear part of the fuselage (represented by the load cases 1 to 25 applied in 4 different x-axis positions in Figure 8 and Figure 9). To obtain the torque load cases, point loads were applied on different spanwise positions of the horizontal tailplane (variation of torque values with a constant shear force applied in 6 different spanwises in each side, represented by the load cases 26 to 35 for increasing left spanwise positions and load cases 36 to 45 for increasing right spanwise positions in Figure 8 and Figure 9). Subsequently two different regression models for each load type were developed, one considering all data and other considering the pure shear and torque data applied for the respective shear and torque load regression models. That is, load cases applied on the rear fuselage were used for the development of the shear regression model and the load cases applied on the horizontal tailplane for the torque regression model. From the comparison of these two models, significant variations of the probable errors of the load estimates and the graphical quality of the fitted models (especially because the bad results from the load cases 6 and 7) were noticed for the shear and torque strain gauge regression models, signaling that considerable influence of torque still affecting the shear regression model (developed with all load cases) and vice versa.

Nevertheless, performing the same comparison for the shear and torque FBG regression models, only small variations are observed, leading to the conclusion that setups with at least three sensors for each load type are able to provide reasonably accurate load regression models (as observed by the improvements obtained from the now good match for the load cases 6 and 7). These small increases in the probable errors of shear and torque estimates from the regression models considering only the relevant data for each load type to that one considering all data mean that the predictors (strain sensors) are powerful enough to decouple

great parts of the interactions between different load types and to represent properly the variation of the load of interest.
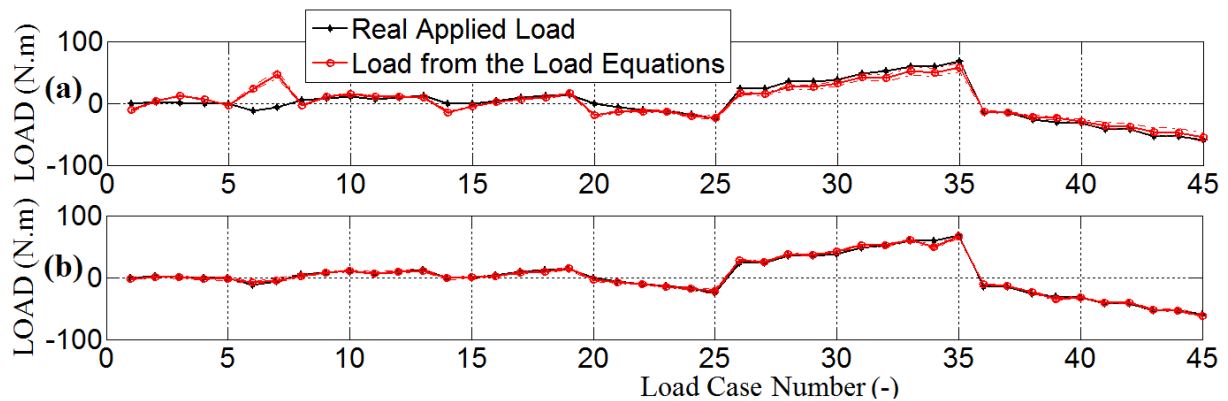


Figure 9: Final torque load model determined from: (a) the strain gauge sensors (2 shear-type and 2 bending-moment-type); (b) the FBG sensors (3 shear-type and 3 bending-moment-type). Using all load cases (all data)

Finally, but not least, it is necessary to point here the importance of the strain sensor redundancy to enable a successful calibration as well as reliable structural heath monitoring. Because without a well-planned redundancy, in case of a strain sensor failure during the flight testing program, big monetary losses could arise due to the interruption of the certification process and need of installation of new sensors followed by the recalibration of all sensors and repetition of flight tests. For the air carriers this faulty SHM could bring impairments in the maintenance processes, which mean additional costs, flight delays and loss of revenue flights. The harsh environment of flight is subject to factors like temperature, humidity and demanding load cycles that can affect the sensitivity and long term stability of these sensors. Subsequently, drifts and degradations could impair their measurements, as noticed in [14]. These issues were addressed in the current work by the considerable number and type diversity of strain sensors installed at various structural locations. Furthermore, this strategic planning of the strain sensor setup will be especially valuable and required for in-flight investigations of the SHM operation regarding reliability, robustness and capability of reconfiguration in face of a sensor failure, as commented in section 2.3.

**4.5 Comparisons between the strain gauge loads models developed from three different optimization criteria: MSE, AIC and optimized AIC**

In order to evaluate different metrics and strategies to develop the most accurate load regression model, a study case was performed using the calibration of the 28 strain gauges installed on the wings, which are distributed in 6 spanwise positions to measure 3 types of load (that is, 18 predictors available for the final load equations). Three different strategies were evaluated for the purpose of selecting a final load regression model from all the possible combinations for these 18 predictors and the constant term ($2^{19} - 1 = 524287$ possibilities):

1. Mean Squared Error (MSE) strategy: the statistical tests were applied eliminating the models with redundant and irrelevant sensors and from this set of potential models the one with the smallest mean squared error (MSE) was selected.

2. Akaike Information Criterion (AIC) strategy: use the minimization of the likelihood function as the sum square error (SSE) penalized by the number of predictors (sensors) in the model to develop the final load regression model.

3. Optimized AIC strategy: similar to AIC strategy, the difference is that engineering judgment and experience were used to select the list of potential predictors that can be the most important to explain the variation of each load of interest.

From the final load regression models as presented in Table 5, an increase in probable errors of load estimates from strategy 1 to strategy 2 can be noticed. However, the significant reduction in the number of sensors required for each load model should be noticed as well. Therefore the strategy 2 demonstrated the effectiveness of the AIC to deal with the bias-variance tradeoff principle and, consequently, to select a model as simple as possible but as complex as necessary. In the current study case, AIC prevented overfitted models, which present inflated variances. Analyzing these results, it was verified that the regression quality metric of adjusted $R^2$ is not as effective as AIC to reach the best model regarding bias-variance tradeoff. For example, considering the changes from strategy 1 to 2 (Table 5), the final load regression model for bending moment at right spanwise 4 presents a reduction of AIC (improvement of the metric of the strategy 2) and number of required predictors (12 to 8 regressors). But this was followed by a reduction of adjusted $R^2$ (degradation of the metric). That is, using the adjusted $R^2$ metric the final load regression models still having redundant sensors.

| Metric of Regression Model Quality | Probable Error of Load Estimate or MSE | Akaike Information Criterion (AIC) | Optimized Akaike Information Criterion (AIC) |
|---|---|---|---|
| Number of predictors | 12 | 8 | 4 |
| Probable Error Load Estimate (N.m) | 6.33152 | 6.36042 | 7.08192 |
| $R^2$ | 0.99892 | 0.99889 | 0.99861 |
| Adjusted-$R^2$ | 0.99887 | 0.99886 | 0.99859 |
| F ratio | 21797.22278 | 32398.50834 | 52251.89109 |
| AIC | 1321.06730 | 1316.03260 | 1337.33804 |
| BIC | 1326.70517 | 1319.79118 | 1339.21733 |

Table 5: Final loads equations for the right wing at the spanwise 4 provided by the strain gauge (SG) sensors

The use of engineering judgment as in the third strategy is essential for at least two reasons. Firstly, it minimizes the workload in load model development by reducing the set of potential combinations. Secondly, an in-depth examination of the final load models can avoid basic errors and check the overall physical meaning of these models, which cannot be performed by an automatized approach. To exemplify the types of errors, in the current calibration, an issue related to the load cases will be addressed: symmetric and asymmetric load cases were planned, but due to restrictions of the available calibration equipment, it was only possible to apply symmetric bending moment load cases. During the load model development through strategies 1 and 2, the final left bending moment models are significantly influenced (biggest coefficient values) by the predictors (strain sensors) of the right wing, what does not correspond with the physical phenomenon that is induced by these load cases. So the limitation of only symmetric bending moments caused errors on the loads model development, due to the situation where those right wing sensors were more able to model the bending moment load cases of the left wing (which are the same load cases applied on the right wing).

In strategy 3 (optimized AIC), each load type potential model considers only the final shear force, bending moment and torque predictors for the corresponding wing (all its three spanwises: e.g. WR1, WR4 and WR6 for the right wing showed in Figure 2) and the final shear force and torque predictors for the opposite wing close to the root (spanwise 1). That is, for the strategy 3, there are twelve possible predictors (eleven final combined strain sensors

plus the intercept) available to develop the load models from 4095 ($2^{12}$ − 1) potential combinations (compared to 524287 ($2^{19}$ − 1) potential combinations for strategies 1 and 2).

In this section the problem about the selection of the most suitable optimization criterion to develop the best loads model was addressed. There is no doubt that engineering judgment is crucial in this process and will probably never be completely replaced.

However, the correct choice of the metric of the optimization criterion is also very important. Methods available in the literature like the T-value [15] could not be suitable, because they could not be effective in eliminating the bad conditioning of the mathematical problem. There is no absolute stop criterion of the irrelevant and redundant sensor elimination process and also no guarantee that the selected direction of elimination will provide the final loads model that encompasses all the physically important predictors. The AIC metric was selected based on its suitable correspondence of the problem physics. The evaluations of the empirical calibration data showed the practical effectiveness of the AIC, which is based on a simple relationship between expected Kullback-Leibler information and Fisher´s maximized log-likelihood function, for developing parsimonious models. Comparing the magnitude of the load equation coefficients of the selected strain sensor predictors with the several strain sensor responses due to the applied loads, it was possible to verify the trustworthy representation of the involved physical phenomenon by the developed loads models. The investigations performed in sections 4.3 and 4.4 about the influence of structural location and number of the strain sensors in the quality of the loads models worked to ratify and justify the technical-based choice of the AIC as the best tested metric in most part of the cases, regarding the sample space of different metrics considered in section 2.3, to develop the loads models. In the current work, the AIC metric worked in a proper way to develop best loads models regarding the trade-off between accuracy and complexity. The architecture of hierarchy (prioritization) between the optimization criteria worked as a feature to drive the process of loads model development based on technical reasons (i.e. engineering evaluation of the quality of the models provided by the different metrics). That is, to select the minimal (optimal) number of the strain sensor predictors that are essential to explain the variation of the considered load.

The penalizing term ($2*p$ in the AIC metric) can certainly be improved and be based on both technical and economic considerations, such as: workload to install a strain sensor, difficulty to access certain aircraft locations, installation time required depending of the type and location of the sensor, cost for different sensor types, accuracy of different technologies and architectures, changes (positive or negative) maintenance-induced costs, additional weight (for sensors, cables, power supply, data acquisition and processing), etc. These new problem variables would lead to a more complex cost function that could be more representative and effective in obtaining the "best possible" loads models for that specific ongoing calibration.

## 4.6 Comparison between the optical fibers and strain gauge loads models

All 46 full bridge strain gauge measurements were recorded concurrently as were the signals for the temperature and strain FBG sensors for the different applied loads. For the right wing only one structural position for the bending moment FBG sensors was selected, namely the junction between the vertical web and the horizontal part of the spar. This position was chosen as it is the main structural component of the wing, where it is expected to obtain the largest bending moment sensitivity. This can be proven by the straightforward relationship between the applied loads and the FBG sensor outputs presented in Figure 10(a). The shear

force FBG sensors are limited to three sensors forming a triangle installed at the wing root in only one structural location, namely the wing shell behind the spar. In the rear fuselage case, three bending moment FBG and three shear force FBG sensors are available. For the bending moment, three locations at the fuselage shell were selected: the upper and lower parts for vertical bending moment measurements, and the left lateral midpoint for lateral bending moment measurements. The fuselage FBG sensors for the shear force type are again arranged in a triangle shape positioned in the superior quadrant of the left fuselage side. In this chordwise, each sensor has a different rotation regarding to the fuselage reference line, in order to measure both shear force and torque influences.
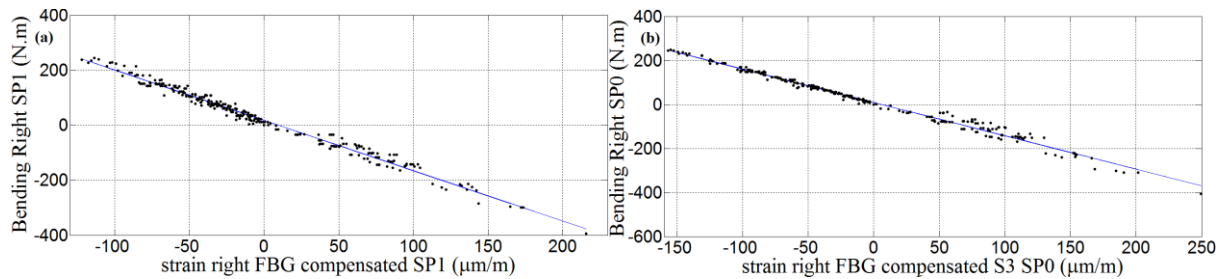


Figure 10: Relationship between the applied bending moments and the strain measurements from: (a) the bending-moment sensor FBG-W1B (spanwise 1); (b) the shear-force sensor FBG-W03S (spanwise 0)

| Load Model | Probable Error of Shear Force (S) Estimate (N) | AIC | Number of Sensors at the corresponding wing spanwise (W) or longitudinal fuselage axis (FUS) | Load Type Sensitivity (S-Shear Force; B-Bending Moment) | Amount of different chordwise positions | Amount of different structural positions |
|---|---|---|---|---|---|---|
| SWR1_FBG | 62.51 | 1894.76 | 1 | B | 1 | 1 |
| SWR1_SG | 7.99 | 1366.32 | 6 | 2 S / 1 $B_1$ / 3 $B_2$ | 3 | 1 $B_1$ / 2 $B_2$ / 2 S |
| SFUS1_FBG | 22.85 | 218.27 | 6 | 3 S / 3 B | 2 | 1 |
| SFUS2_SG | 68.72 | 256.68 | 4 | 2 S / 1 $B_1$ / 1 $B_2$ | 1 | 1 |

**\* SG: strain gauges; FBG: Fiber Bragg Gratings or simply optical fibers; SFUS1: loads model for shear force at the rear fuselage in the station 1 (150 mm behind the ring frame); SFUS2: loads model for shear force at the rear fuselage in the station 2 (250 mm behind the ring frame); SWR1: loads model for shear force at the right wing spanwise 1.**
**\*\* $B_1$ and $B_2$ represent two different types of strain gauge sensors for bending moment measurements, respectively, EA-06-250MQ-350 and CEA-06-125WT-120 types (see Figure 2 and Figure 3).**

Table 6: Comparisons of the probable errors of load estimates and AIC values from the final calibration loads models obtained from the FBG and strain gauge sensors installed on the wing and fuselage, considering all data

The load models from the FBG sensors can be compared with those from the strain gauge sensors at the positions where there are both strain gauges and FBG sensors, namely: right wing spanwises 1, 4 and 6, and rear fuselage (shown in Figure 12(a)). Table 6 summarizes the comparisons between the loads models from FBG and strain gauge sensors installed at the rear fuselage and right wing. Considering the wing final loads models, Table 6 provides a good summary of the results that support the conclusion that the strain gauge sensors can be used in the development of more accurate loads regression models in comparison with those from the FBG sensors. However these comparisons are not based on the same level of equivalency, because in the case of the strain gauge models the number of sensors positioned in different chordwise and structural positions is significantly superior. So the strain gauge network of information is more comprehensive and improves the capability to develop loads models with an improved quality. Because complex instrumentation architectures, like these composed by the strain gauges, are able to transform the sensor measurements constituted by mixed loads types into pure loads measurements. However, the fuselage final loads models presented in Table 6 aid to achieve the final conclusion about the FBG technology validation. From these results of probable errors of load estimates and AIC values, the developed FBG loads regression models present a better accuracy than those from the strain gauge sensors. In

the case of the rear fuselage, there is an inversion regarding the situation of the right wing loads models. Now FBG loads models are developed based on a largest number of sensors than those available of strain gauges.
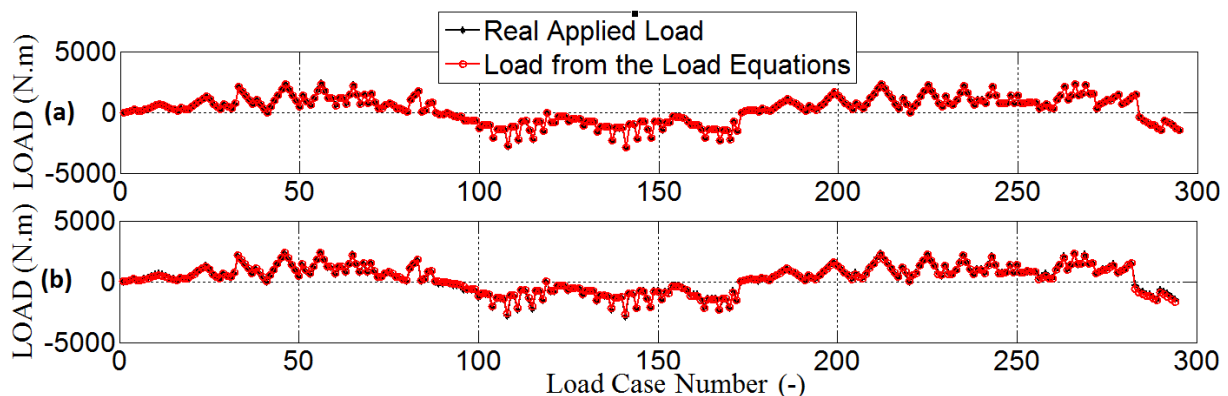


Figure 11: Comparison between the applied and the fitted bending moments provided by: (a) the strain gauge sensors at the right wing spanwise 1; (b) the FBG sensors at the right wing spanwise 1

Moreover the plots of the strain measurements from the strain gauges against the applied bending moments show considerably similarity with those from the FBG. Figure 10(a) presents a bigger scatter of the FBG-W1B results than those from Figure 7(a) (SG-WR1B1). However the results from Figure 10(a) show smaller scatter than those from Figure 7(b) (SG-WR1B2) and Figure 7(c) (SG-WR1B3). The explanation is that the sensor SG-WR1B1 is installed on the upper and lower horizontal part of the double-T-spars, while the sensor FBG-W1B is installed only at the intersection between the vertical and horizontal parts of the double-T-spars, which provided a limited sensitivity for this FBG sensor. However the sensors SG-WR1B2 and SG-WR1B3 are installed in a similar way as the sensor FBG-W1B, that is, only in one region of the horizontal part of the wing spar. In this case, one can notice that, considering the same installation architecture the FBG sensor presents improved bending moment sensitivity. All these results validate the FBG strain measurements with the strain gauge measurements for the same structural positions. The information provided by the FBG sensors is sufficient to develop accurate loads models. The level of accuracy of these models is in great part a matter of strategic planning of the instrumentation architecture. The number and types of sensors positioned in different chordwise and structural components are two of the key points for a successful loads calibration. All these conclusions are confirmed by the plots of the fitted loads against the applied loads for the strain gauge and FBG sensors, given in Figure 11(a) and Figure 11(b), respectively.

**4.7 Sources of errors and inaccuracies for the loads regression models development**

From the results obtained in this particular calibration, it is evident that the methodology is practicable. Some improvements for the developed loads models can certainly be achieved. For example, scatter of the strain sensor outputs around their linear relationship with the applied bending moments are noticeable, shown in Figure 10(a) and Figure 10(b) and also by the plots of the influence coefficients. To explain these inaccuracies, practical limitations during the calibration performance caused some sources of errors, such as:

1. The load cases applied on the wings and fuselage: sand bags were used that have dimensions of 30 x 60 cm, and metal bars of 5 x 10 cm for the horizontal tail. Considering the limitation of the exact position determination of the load application, significant errors

can be made, for example, considering reasonable inaccuracies of the applied loads position of the order of the half of smallest dimensions (i.e. 15 and 2.5 cm, respectively).

2. The calibration tests were performed inside of a closed hangar in order to obtain a well stabilized condition before the recording of the strain sensor measurements. However, during several test points, the hangar doors were opened and the wind slightly disturbed the aircraft, impairing the quality of the measurements.

3. Due to a missing of a suitable support on the wing root to stabilize and level the aircraft, it was used a support position at an outboard wing spanwise. However, the sailplane wing is very flexible and this is not a proper position for this stabilizing support, because the wing can touch this support and transfer part of the applied load.

4. Due to restriction of unknown structural limits of the sailplane components, only few load cases with relatively low magnitude values were applied. This conservative approach impaired the quality and the proper development of the loads models.

5. The sand bags lost some grains during the calibration process. Resulting in a slight variation of weight of the sand bags that influences the accuracy of the applied loads and thereby of the developed loads models.

6. The limitation of number of strain sensor types in certain positions degraded the quality and accuracy of the obtained loads models. 175 load cases were applied on the horizontal tail, nevertheless, the predictions of the left side loads models did not present a good fit with them due to the small number of available predictors. Comparing these loads models with the similar models in the right side, the quality differences are noticeable. This ratifies the conclusions of the item 4.4 about the necessary minimal number of each sensor type.

7. Several load cases are applied considerably close to spanwise 4 of the wings, the loads models at this position present some inaccuracies, derived from the fact that in real applications the strain gauges are affected by loads acting inboard regions near to the sensor position. Moreover, due to the large application surfaces of the loads, sometimes only part of these loads are measured by the sensors, because of part of their applications were acting in the inboard region, causing errors in the loads regression models. The inclusion of an uncertainty parameter in the loads regression identification could lead to erroneous coefficients for the loads models, with nonphysical meaning.

8. Due to the hardware restriction in applying downward loads at the rear fuselage, the fuselage loads models are limited to predict only upward loads.

9. In some structural components, the number of strain sensors installed was limited and not enough in order to ensure an adequate redundancy for the objectives addressed in sections 2.3 and 4.4. This limits the reliability of the developed load models and restrains desired capabilities of the SHM. Additional in-flight investigations of the sensor operation under influencing flight factors (e.g. temperature) are required for the proper evaluation of the loads models regarding the all the issues considered during the instrumentation architecture design.

It should be kept in mind that the main objective of this work was to develop a methodology to build adequate loads monitoring models applicable with limited budget, and

straightforward and accessible even for small airplanes. More expensive setups or equipment would eliminate or drastically reduce most of the aforementioned sources of uncertainties.

## 4.8 First insight into the quality of the obtained load regression models

Structural loads are composed by inertia and aerodynamic loads. Changes in strain sensor responses from the ground to flight at 1 g are exclusively proportional to the aerodynamic load. With the sailplane undergoing accelerating flight conditions the loads measured by the strain sensors are structural loads, which should be corrected by the inertia loads if the interests are the aerodynamic loads. Therefore, to develop a proper aerodynamic loads model it is essential to know the inertia of the structural components, which will be monitored. In order to anticipate this future need, each part of the wings (outer and inner wings) was removed one by one, allowing the determination of their individual CG positions (x and y axes) and masses. Considering that this data was available, it will be used here to evaluate the quality of the developed load equations.

Taking into account this objective, these direct measurements were compared with the predictions from the developed loads models, as shown in Table 7. Figure 12(a), Figure 12(b), Figure 12(c) and Figure 12(d) show the sailplane configurations with the sensor, whose measurements can be still be used. Indeed, applying the strain gauge and FBG final loads regression models to the measured load reference conditions with all aircraft structural components disassembled and supported in a level condition, the masses of these wing components can also be deduced from the changes in the measured loads and compared with the direct mass measurements, as given by the respective differences highlighted in red color in Table 7. The good match between the deduced and measured masses reinforces the confidence level that both values were determined with adequate precision. Moreover, the small differences between the measurements and the values predicted from the loads regression models provided by both strain gauge and FBG sensors are an additional indication of the accuracy and quality of the calibrated models.
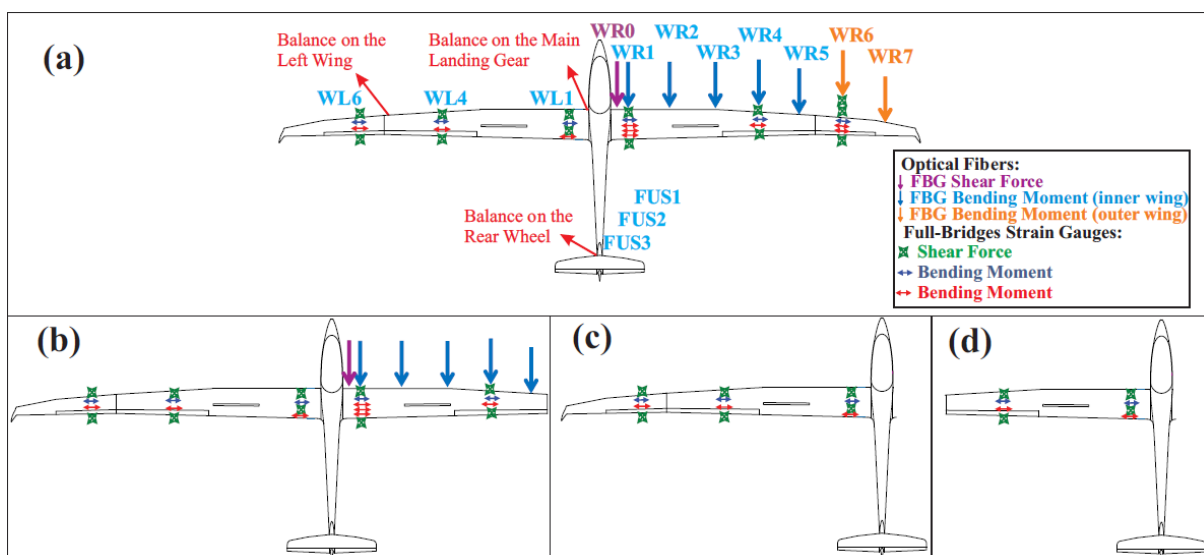


Figure 12: (a) Sailplane instrumentation for strain measurements; Sailplane weighing: (b) determination of the CG positions of the right outer wing; (c) determination of the CG positions of the right inner wing as well as of the whole right and left wings; (d) determination of the CG positions of the left inner and outer wings

| | Spanwise | -6 | -4 | -1 | 1 | 4 | 6 |
|---|---|---|---|---|---|---|---|
| **Mass of the wing outboard part of the given spanwise from the measurements and from the shear force models** | Value measured in the sailplane weighing (kg) | 7.00 | 26.22 | 79.24 | 79.67 | 26.22 | 7.00 |
| | Value calculated from the SG shear force model (kg) | 6.61 | 26.89 | 85.58 | 87.09 | 28.02 | 5.21 |
| | Difference (%) | -5.52 | 2.56 | 8.01 | 9.32 | 6.87 | -25.49 |
| | Value calculated from the FBG shear force model (kg) | - | - | - | 83.90 | 22.91 | - |
| | Difference (%) | - | - | - | 5.31 | -12.63 | - |
| **Lateral CG (y-axis) of the wing outboard part of the given spanwise from the measurements and from the bending moment models** | Value measured in the sailplane weighing (mm) | -7897.23 | -6004.05 | -3205.31 | 3205.31 | 6004.05 | 7897.23 |
| | Value calculated from the SG bending moment model (mm) | -7780.33 | -6167.92 | -3213.66 | 3118.33 | 6155.82 | 7753.80 |
| | Difference (%) | -1.48 | 2.73 | 0.26 | -2.71 | 2.53 | -1.82 |
| | Value calculated from the FBG bending moment model (mm) | - | - | - | 2902.83 | 6254.89 | - |
| | Difference (%) | - | - | - | -9.44 | 4.18 | - |
| **Longitudinal CG (x-axis) of the wing outboard part of the given spanwise from the measurements and from the torque models** | Value measured in the sailplane weighing (mm) | 549.60 | 400.79 | 387.15 | 387.15 | 400.79 | 549.60 |
| | Value calculated from the SG torque model (mm) | 718.80 | 465.30 | 352.91 | 371.39 | 447.23 | 587.33 |
| | Difference (%) | 30.79 | 16.10 | -8.84 | -4.07 | 11.59 | 6.86 |
| | Value calculated from the FBG torque model (mm) | - | - | - | 392.68 | 458.94 | - |
| | Difference (%) | - | - | - | 1.43 | 14.51 | - |

Table 7: Comparisons between the measured values of mass and CG positions (x and y axes from the leading edge of the wing root and centerline, respectively) of each wing part outboard of the corresponding spanwise locations, where the strain gauge and FBG sensors are installed, and those values deduced by the loads regression models developed from the strain gauge (SG) and FBG sensors

Specifically in order to validate the developed loads regression models, point and distributed loads different to those used for the preliminary and final calibrations were applied to the aircraft structural components. The distributed check loads are used to simulate loads in flight. The comparisons between the applied loads and the respective predictions from the developed models for bending moment on the right wing spanwise 1 from the strain gauge and FBG sensors are given in Figure 13(a) and Figure 13(b), respectively. Similar results are obtained for the strain gauge and FBG sensors installed at the other wing, rear fuselage and horizontal tailplane positions. From the analyses of the differences between the applied and calculated check loads, and from the values of probable errors of the load estimates, the quality of the developed load models can be assessed from the different used strain sensors.
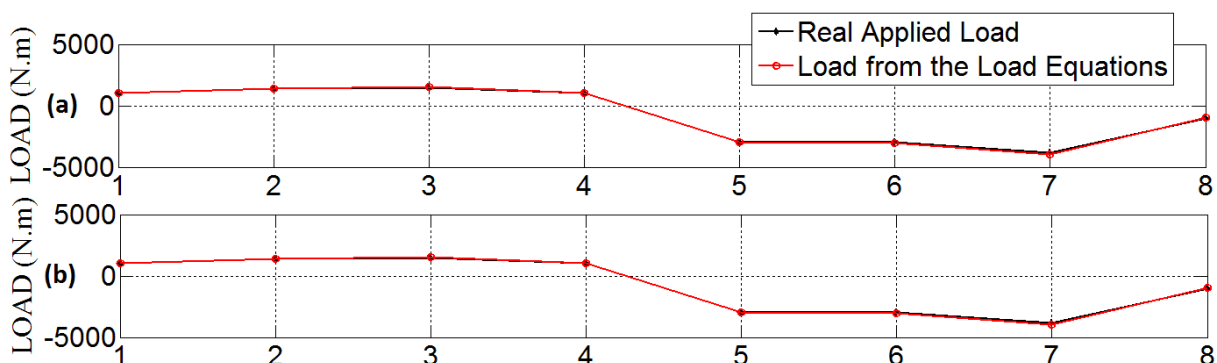


Figure 13: Check-loads validation of the: (a) strain gauge; (b) FBG bending moment models at the spanwise 1

In general, considering the restricted hardware (material support) used in this calibration and the sources of errors addressed in section 4.7, the developed loads models showed suitable quality and accuracy, as can be verified by the results presented in this section. In spite of the

presence of quite a few sources for inaccuracies in the experimental setup that impact the final load models, the results obtained in this application are still very satisfying and in line with the expectations.

## 5 SUMMARY AND FUTURE WORK

The developed load models show promising quality to fulfill the development of the integrated model of structural, loads and flexible aircraft flight dynamics, even for the application of the presented calibration methodology to a sailplane with a limited budget and limited material support. Future work will consider the use of the obtained load regression models with the flight test data gathered during the Discus-2c flight test program that took place in the second semester of 2014 [16]. The presented calibration methodology and the resultant loads regression models are essential parts of a project with the objective to contribute to the development and consolidation of structural health monitoring (SHM) technologies with regards to feasibility and reliability in an embedded, integrated system for multi-site sensing of flexible aircraft structures. The results presented in this paper and detailed in [17] provide clearance to move forward to the next steps of the mentioned project. As calibrated strain sensors will work to support the development and validation of the local aerodynamic load models identified from the flight parameters. A longer-term goal of these load models will be the design of the SHM system running onboard during every flight and during the entire aircraft lifecycle.

## 6 ACKNOWLEDGMENTS

## 7 REFERENCES

[1]   CS-25, Certification Specifications and Acceptable Means of Compliance for Large Airplanes, EASA, 2012, *http://www.easa.eu.int/home/index.html*.

[2]   Wright, J. R., Cooper, J. E., Introduction to Aircraft Aeroelasticity and Loads, *John Wiley & Sons*, Ltd, Chichester, 2007.

[3]   Skopinski, T. H., Aiken, W. S., Jr., Huston, W. B., Calibration of Strain-Gage Installations in Aircraft Structures for the Measurement of Flight Loads, *NACA Report 1178*, 1954.

[4]   Jategaonkar, R. V., Flight Vehicle System Identification – A Time Domain Methodology, Progress in Astronautics and Aeronautics, Volume 216, AIAA, 2006.

[5]   James, S. W., Chapter 5 – Fibre Bragg Grating Strain Measurement, Handbook of Advanced In-Flight Measurement Techniques, *AIM2 Advanced Flight Testing Workshop*, BoD – Books on Demand, Norderstedt, 2013.

[6]   Eisenhauer, J. G., Regression through the Origin, *Teaching Statistics*, volume 25, no. 3, pages 76-80, 2003.

[7]   Yan, X.Y, Su, X.G., Linear Regression Analysis: Theory and Computing, *World Scientific Publishing Co*, 2009.

[8]   Burnham, K. P., Anderson, D. R., Multimodel inference understanding AIC and BIC in model selection, Sociological methods & research, v. 33, n. 2, p. 261-304, 2004.

[9]   de Leeuw, J., Introduction to Akaike (1973) information theory and an extension of the maximum likelihood principle, p. 599-609 in S. Kotz, and N. L. Johnson (editors) Breakthroughs in statistics, v. 1, Springer-Verlag, New York, 1992.

[10]  Viana, M. V. P., Flight-Loads Sensor Calibration Procedure for DLR Discus-2c Sailplane, *DLR internal document*, Braunschweig, June 2013.

[11]  Sauerbrei, W., Royston, P., Binder, H., Selection of important variables and determination of functional form for continuous predictors in multivariable model building, *Statistics in medicine 26.30*: 5512-5528, 2007.

[12]  Kvålseth T.O., Cautionary note about R², *The American Statistician*, volume 39, no. 4, pages 279–285, 1985.

[13]  Lokos, W. A., Olney, C. D., Chen, T., Crawford, N. D., Stauf, R., Reichenbach, E. Y., Strain Gage Loads Calibration Testing of the Active Aeroelastic Wing F/A-18 Aircraft, NASA/TM-2002-210726, 2002.

[14]  Reijerkerk, M. J., Aeroelastic Model Identification of Winglet Loads from Flight Test Data, Ph.D. Thesis, Delft University of Technology, 2008.

[15]  Hovell, P. B., Webber, D. A., Roberts, T. A., The Interpretation of Strain Measurements for Flight Load Determination, C.P. No. 839, Her Majesty's Stationery Office, London, 1966.

[16]  Viana, M. V. P., Flight Test Program – Integrated Model of Structural, Loads and Flight Dynamics for DLR Discus-2c Sailplane System Identification, *DLR internal document*, Braunschweig, November 2013.

[17]  Viana, M. V. P., Sensor Calibration for Calculation of Loads on a Flexible Aircraft – Research Project: Integrated Model of Structural, Loads and Flight Dynamics for DLR Discus-2c Sailplane System Identification, DLR internal report (under approval process), Braunschweig, December 2014.

## 8 COPYRIGHT STATEMENT